Algerian Journal of Research and Technology
https://doi.org/10.58681/ajrt.24080105
A.J.R.T Volume 8 (N°2) (2024) 42 - 56

Novel Inorganic-Organic Heterojunction Solar Cell based Pt/$CuSbS_2$/Abs/ZnO/FTO Perovskite Using Two MAPI and FAPI Absorbent Materials

K.Dris[1], M.Benhaliliba[2]*

[1]*Film Device Fabrication-Characterization and Application FDFCA Research Group USTOMB, 31130 Oran, Algeria*
[2]*Laboratoire d'études physiques des matériaux Université des Sciences et de la Technologie d'Oran Mohamed Boudiaf USTO-MB, El M'naouer, BP 1505, 31000 Oran, Algeria*

Corresponding author: mbenhaliliba@gmail.com

Received.December 21, 2023. Accepted. March15, 2024. Published May 15, 2024.

DOI: https://doi.org/10.58681/ajrt.24080105

Abstract. In this paper, three perovskite solar cell (PSCs) configurations were proposed and compared in order to improve their performance. The first suggested cell consists of six materials arranged in the sequence FTO/ETL/FAPI/MAPI/HTL/Pt, comprising two active sub-layers, FAPI and MAPI. The performance of this double-active-layer cell was compared to that of two single-layer cells, each containing an only active layer of perovskite material used in proposed cell, with FTO/ETL/MAPI/HTL/Pt and FTO/ETL/FAPI/HTL/Pt configurations. The simulations were conducted using SCAPS-1D software. The study investigated the impact of active layer thickness, doping density, and defect density on J-V characteristics for each cell, comparing the results obtained at the same time. Additionally, the defects density in interfaces: MAPI/HTL, FAPI/MAPI and ETL/FAPI of the double-absorber cell were optimized. The best results were achieved by the double-layer cell with thickness of 1500 nm, defect density of 10^{10} cm^{-3} and doping density of 10^{20} cm^{-3} for FAPI and MAPI materials. The optimized cell exhibited Voc = 1.41 V, Jsc = 27.88 mA/cm^2, FF = 90.12 %, and PCE = 35.46 %.

Keywords. PSC; $CH_3NH_3PbI_3$; $HC(NH_2)_2PbI_3$; Double-absorber; Thickness ; Acceptor density; Defect density.

INTRODUCTION

Perovskite solar cells (PSCs) based on organometallic halides stand out as a unique and advanced technology within the realm of solar cells. These cells offer numerous benefits, including a straightforward manufacturing process, exceptional photovoltaic performance, and high efficiency. They have a broad range of cost-effective applications, making them a promising option in the field of solar energy (Daskeviciute-geguziene et al., 2023).

The inception of PSCs dates back to 2009 when researcher Kojima and colleagues first introduced them. Since then, PSCs have made remarkable progress, with their efficiency increasing from 3.81% in 2009 to 26.1% in 2021, positioning them as strong contenders against traditional solar cells (Pochont et al., 2022; Kojima et al., 2009).

The core component of most perovskite cells is calcium titanate ($CaTiO_3$), which gave rise to the term "perovskite" initially referring to this mineral and later encompassing all oxides sharing the ABO3 chemical formula and structure, where (A, B) represent cations with a notable size difference (Assirey, 2019).

The prevalent lead-based perovskites in PSCs are methylammonium lead iodide (MAPI) and formamidine lead iodide (FAPI) (Pastuszak and Węgierek, 2022). These materials exhibit favorable optical and electrical properties, including a band gap ranging from 1.3 to 2.2 eV, extended diffusion times, low exciton binding energies, high absorption coefficients, and even ferroelectric behavior (Chowdhury et al., 2023; Husainat et al., 2019).

While single-perovskite structured PSCs have demonstrated high efficiency, they face challenges such as limited lifespan, structural degradation, inefficient charge transport, and difficulties in large-scale production (Zhang et al., 2019; Lye et al., 2023). To address these issues, various research endeavors have focused on enhancing PSC performance. Some studies have explored materials for electron and hole transport layers (ETM and HTM) to boost efficiency (Zhang et al., 2022; Huang et al., 2022; Al-Mousoi et al., 2022), while others have investigated alternative perovskite materials like tin-based for the active layer to improve overall cell performance (Yang et al., 2023; Ke et al., 2019).

We propose a perovskite solar cell configuration as follows: FTO/ZnO/$HC(NH_2)_2PbI_3$/$CH_3NH_3PbI_3$/$CuSbS_2$/Pt characterized by its double-layered active structure utilizing the perovskite $HC(NH_2)_2PbI_3$ and $CH_3NH_3PbI_3$.

To validate the performance of this configuration, we studied two single-ply perovskite cells, each containing a single absorber material layer, with FTO/ZnO/MAPI/$CuSbS_2$/Pt and FTO/ZnO/FAPI/$CuSbS_2$/Pt configurations.

The materials in the absorber of our proposed cell exhibit energy band alignments that enhance electron separation and transport efficiency. ZnO was selected as ETM (Bouazizi et al., 2022) and $CuSbS_2$ was employed as HTM (Mushtaq et al., 2023). Pt was selected as the back contact and FTO as the front contact.

STRUCTURE

This study investigates three types of perovskite solar cells, which share the same front and rear contacts and HTL and ETL transport layers, but differ in their absorbent layers. The configurations of these models are FTO/ZnO/MAPI/$CuSbS_2$/Pt and FTO/ZnO/FAPI/$CuSbS_2$/Pt, and FTO/ZnO/FAPI/MAPI/$CuSbS_2$/Pt (Fig.1, a-b-c),

respectively. The focus is on the third cell, while the other two serve as a basis for comparison and validation of the best performance among the three models.

Pt is used as a rear contact and FTO (fluorinated tin oxide), a transparent conductive material, is used as front contact. Titanium dioxide (TiO_2) is a notable electron transport material in perovskite technology, but its high-temperature deposition poses a challenge in commercialization. To address this, researchers have explored various materials for ETL in PSCs, including different ETMs (Zahran and Hawash, 2022; Sumbel et al., 2023; Rai et al., 2020; Lakhdar and Hima, 2020; Chabri et al., 2023). ZnO was chosen as the ETL for the cells due to its transport properties (Koné et al., 2023; Zheng et al., 2019).

Copper antimony sulphide ($CuSbS_2$) can serve as both an active layer and a hole transport layer (HTL) (Puente-López and Pal, 2023; Noman et al., 2023). This material was chosen as the HTL for the cells due to its band gap of 1.58 eV and low melting temperature of 551°C (Mushtaq et al., 2023; Chalapathi et al., 2023).

The active layer consists of two materials, $HC(NH_2)_2PbI_3$ (FAPI) and $CH_3NH_3PbI_3$ (MAPI), due to their attractive properties such as high mobility of charge carriers, very high absorption coefficient, and long charge diffusion length (Idrissi et al., 2021; Baral et al., 2023).

The FAPI material has a large ionic radius, long charge diffusion lengths, and a high phase transition temperature, while the MAPI material has panchromatic absorption from visible to near-infrared, a direct forbidden optical band of 1.55 eV, a high absorption coefficient, high dielectric constant, and long charge diffusion time (Yousuf and Qazi, 2021; Qirong et al., 2022).

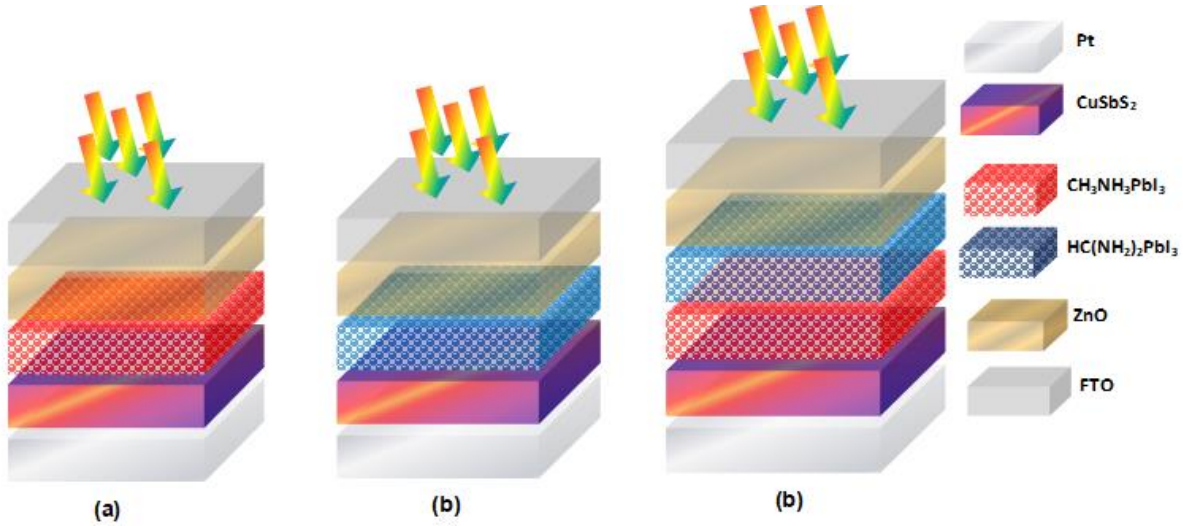

Fig.1. The structure for different cells: (a) FTO/ZnO/MAPI/$CuSbS_2$/Pt, (b) FTO/ZnO/FAPI/$CuSbS_2$/Pt, and (c) FTO/ZnO/FAPI/MAPI/$CuSbS_2$/Pt.

SCAPS 1D SIMULATION PROGRAM

The study used a one-dimensional numerical modeling software called "SCAPS-1D" (Solar Cell Capacitance Simulator - One Dimension) version 3.3.07. The program was developed by Marc Burgelman and his team at Ghent University in Belgium, specifically for the simulation of solar cells. It is capable of analyzing various parameters such as band structure,

recombination rate, generation rate and device characteristics (I-V, C-V, C-f). SCAPS-1D helps understand the working mechanism of solar cells by solving equations related to hole and electron continuity as well as Poisson's equation (Mushtaq et al., 2023).
The Poisson equation (Mushtaq et al., 2023):

$$-\frac{\partial}{\partial x}\left[-\varepsilon\frac{\partial V}{\partial x}\right]=q[p-n+N_D^+-N_A^-+p_t-n_t] \quad (1)$$

The electron continuity equation(Mushtaq et al. 2023) :

$$\frac{\partial n}{\partial t}=G_n-R_n+\frac{1}{q}\frac{\partial J_n}{\partial x} \quad (2)$$

The hole continuity equation(Mushtaq et al., 2023):

$$\frac{\partial P}{\partial t}=\frac{1}{q}\frac{\partial J_P}{\partial x}+G_P-R_P \quad (3)$$

With: ε denotes the dielectric permeability of the material. q represents the charge of an electron. V signifies the potential within the material. p stands for the concentration of free holes. n refers to the concentration of free electrons. p_t denotes the density of hole traps. n_t signifies the density of electron traps. N_D^+ indicates the concentration of ionized donors. N_A^- represents the concentration of ionized acceptors. J_n represents the current density of electrons. J_p denotes the current density of holes. *Rn* denotes the rate of electron recombination. *Rp* represents the rate of hole recombination. G_n signifies the rate of electron generation. *Gp* represents the rate of hole generation.

SIMULATION PARAMETERS

Table 1 presents the physical parameters of FTO, $CuSbS_2$ (HTL), ZnO (ETL), FAPI and MAPI. The simulation conditions used were those of AM1.5G solar spectrum, T = 300 K, and P = 1000 W/m^2, for our simulations (Puente-López and Pal, 2023).

Table 1. Input Parameters for Materials in the Device Simulation.

Parameter	$CuSbS_2$	MAPI	FAPI	ZnO	FTO
Band gap (eV)	1.58	1.55	1.51	3.3	3.5
Thickness (nm)	100	Variable	variable	100	100
Dielectric permittivity	14.6	30	6.6	9	9
Electron affinity (eV)	4.2	3.9	4	4.1	4
VB effective density of states (1/cm^3)	10^{19}	10^{18}	2.9×10^{18}	10^{19}	1.8×10^{19}
CB effective density of states (1/cm^3)	2×10^{18}	2.25×10^{18}	1.2×10^{19}	4×10^{18}	2.2×10^{18}
Hole thermal velocity (cm/s)	10^7	10^7	10^7	10^7	10^7
Electron thermal velocity (cm/s)	10^7	10^7	10^7	10^7	10^7
Hole mobility (cm^2/Vs)	49	2.2	1.8	25	10
Electron mobility (cm^2/Vs)	49	2.2	2.7	100	20
Shallow uniform acceptor density	1.38×10^{18}	10^{18}	10^{19}	0	0

$N_A(1/cm^3)$					
Shallow uniform donor density N_D $(1/cm^3)$	0	0	0	10^{20}	2×10^{19}
N_t $(1/cm^3)$ total	10^{14}	10^{12}	4×10^{13}	10^{15}	10^{16}
Reference	(Mushtaq et al., 2023 ; Shivesh et., 2022)	(Thakur et al., 2022; Qirong et al., 2022 ; Husainat et al., 2019)	(Karthick et al., 2020)	(Bouaziz i et al., 2022 ; Qasim et al., 2022)	(Sumbel et al., 2023)

RESULTS OF SIMULATION STUDIES

For the initial phase, a comparative analysis was undertaken involving three solar cell models, with the objective of optimizing the thickness, defect density N_t, and doping density N_A within the active layer of each model. As the investigation progressed, the focus shifted towards a more in-depth examination of the third model, specifically investigating how the defect density at the interfaces impacts the overall cell performance.

IMPROVED ABSORBENT THICKNESS

Investigating the impact of the active thickness is crucial for enhancing solar cell efficiency. The active layer plays a pivotal role in determining the cell's light response, necessitating precise adjustment of its thickness to optimize light absorption. An excessively thick active layer can lead to poor performance due to increased serial resistance and recombination rates. Conversely, an overly thin active layer may result in fewer electron-hole pairs being generated as a majority of incident photons pass through (Raj et al., 2023; Ravidas et al., 2023).

Numerous studies, such as those by (De Los Santos et al., 2020; Bag et al., 2020), (Yousuf and Qazi, 2021; Dixit et al., 2022), have focused on optimizing the absorber layer, particularly its thickness. To determine the optimal thickness, we varied the active layer thickness of each cell from 100 to 1500 nm while keeping other parameters constant (with simultaneous adjustment of the two active layer materials, FAPI/MAPI, for the third cell to simplify the study). The results, depicted in figure 3, illustrate that increasing the active layer thickness enhances the J-V characteristics across all three models.

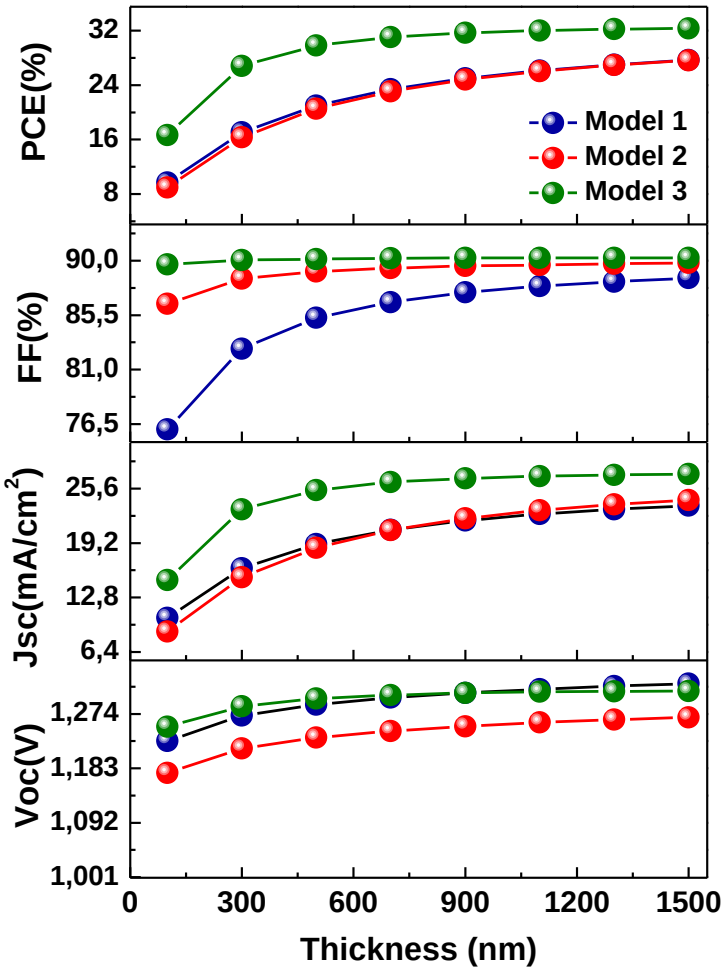

Fig.2. Illustrates the impact of varying the thickness of the active layer on J-V curves of three distinct models.

For the first model, as the MAPI active layer thickness increased from 100 to 700 nm, the FF and PCE values exhibited rapid growth, reaching maximum values at 1500 nm. Similarly, the second model showed significant improvements in Voc, Jsc, FF, and PCE with increasing FAPI layer thickness. The third model displayed notable enhancements in Voc, Jsc, and PCE with increasing FAPI/MAPI double layer thickness, with FF showing a slight increase.

The performance improvements observed with thicker active layers can be attributed to increased photon absorption and subsequent generation of charge carriers (Hima et al., 2019; Aseena et al., 2021).

Comparing the results, the double perovskite cell exhibited superior J-V characteristics. All three cells demonstrated optimal performance at a thickness of 1500 nm, which was selected for subsequent simulations.

OPTIMIZATION OF THE DOPING DENSITY IN THE ABSORBER OF THE THREE MODELS

Numerous research studies have highlighted the significance of optimizing the doping density within the active layer as a critical factor in enhancing the performance of perovskite solar cells (Rono et al., 2021; Noman et al., 2023; Puente-López and Pal, 2023). To determine the ideal doping density for the absorber in each model, simulations were conducted across a range of 10^{10} to 10^{20} cm^{-3} for all three models. These simulations were performed while maintaining the parameters outlined in Table 1 constant and utilizing the previously determined optimal active layer thickness of 1500 nm for each cell. Figure 3 illustrates the J-V characteristics in relation to the variation in doping density within the absorber for the three cells.

Optimizing the doping density in the active layer is crucial for enhancing the efficiency of perovskite solar cells (Rono et al., 2021; Noman et al., 2023; Puente-López and Pal, 2023). Simulations were conducted for the doping density of the absorber, ranging from 10^{10} to 10^{20} cm^{-3} for the three models. The simulations were performed while keeping all parameters constant and using the optimal thickness of the active layer for each cell (1500 nm).

The results revealed that for the first and second models, the variation in doping density from 10^{10} to 10^{16} cm^{-3} had no significant impact on the Voc and Jsc. However, beyond 10^{16} cm^{-3}, the Voc increased significantly with the increase in doping density, while the Jsc decreased rapidly. For the third model, the Voc and Jsc remained almost constant for doping densities from 10^{10} to 10^{16} cm^{-3}, but beyond the latter, the Voc began to increase, while the Jsc showed a slight decrease.

The FF and PCE for the first and second models showed a slight decrease for doping densities from 10^{10} to 10^{14} cm^{-3}, and then increased slightly for densities greater than 10^{16} cm^{-3}. The third model showed a rapid increase in FF and PCE for densities greater than 10^{16} cm^{-3}. The increase in electric field and recombination rate at the ZnO/FAPI interface with increasing doping density in the third model led to improved separation of charge carriers and higher efficiency (Fig. 4) (Bag et al., 2020). The optimum density of the absorbing layer for the three cells was found to be 10^{20} cm^{-3}, which was used for subsequent simulations.

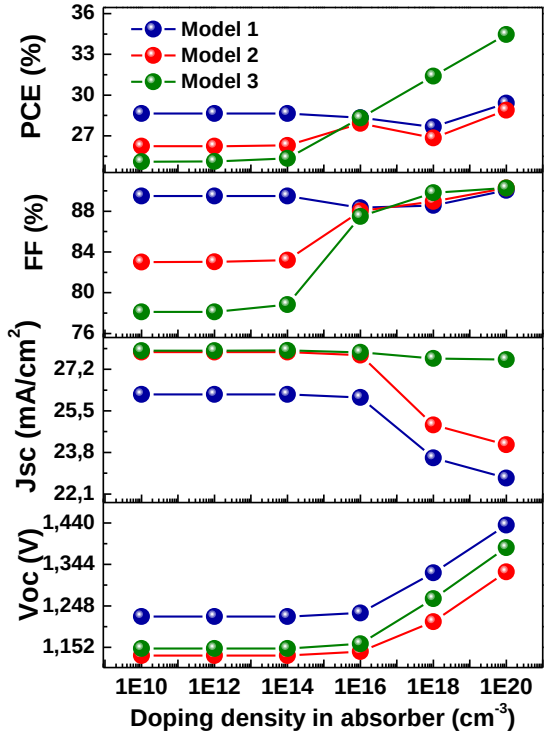

Fig.3. Influence of doping density in active layer of each solar cell on J-V characteristics.

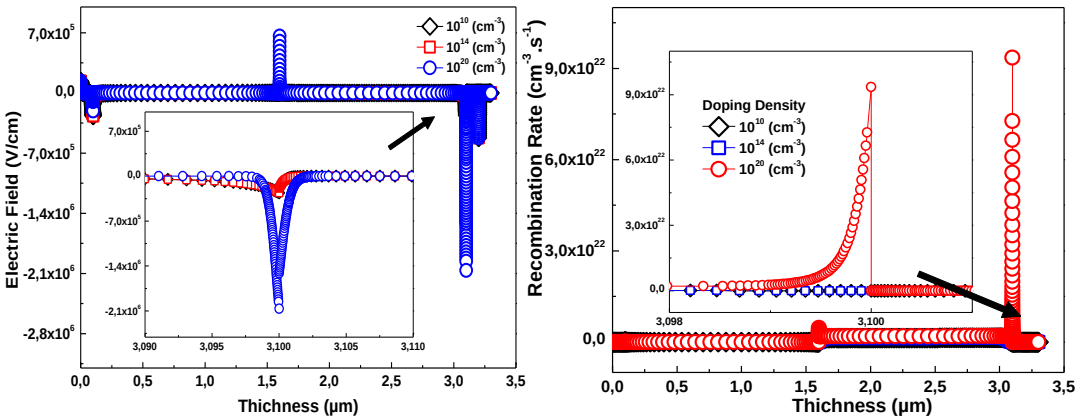

Fig.4. (a) Changes in the Electric field in relation to the doping density within the absorber of the third cell labeled FTO/ETL/FAPI/MAPI/HTL/Pt (b) The variability of recombination rate corresponding to the doping density within the absorber of third cell.

THE EFFECT OF THE DEFECT DENSITY IN THE ACTIVE LAYER

The impact of defect density in the active layer on the performance of perovskite solar cells (PSCs) was investigated by varying the N_t defect density from 10^{11} cm^{-3} to 10^{19} cm^{-3} for each model (Bera et al., 2022). Figure 5 (a) illustrates the effect of defect density on the J-V characteristics of each model. For the first cell utilizing MAPI absorber, PV parameters remained stable below 10^{13} cm^{-3}, then decreased significantly beyond this threshold. The second cell with FAPI absorber exhibited similar trends, maintaining stable parameters up to 10^{13} cm^{-3} before declining rapidly. In contrast, the third cell with MAPI/FAPI absorber maintained stable parameters up to 10^{13} cm^{-3} before experiencing a rapid decline. Figure 5 (b) demonstrates the increase in recombination rates with higher defect densities in the third model, leading to decreased cell performance.

Comparing the results, the double perovskite cell showed the best performance, with optimal parameters achieved at a defect density of 10^{13} cm^{-3}: Voc of 1.41 V, Jsc of 27.88 mA/cm^2, FF of 90.11%, and PCE of 35.36%. These findings highlight the challenge of achieving experimentally low defect densities and emphasize the importance of selecting an optimal defect density for improved cell performance. The results underscore the superior performance of the double perovskite cell, leading to a focus on further study of this particular model.

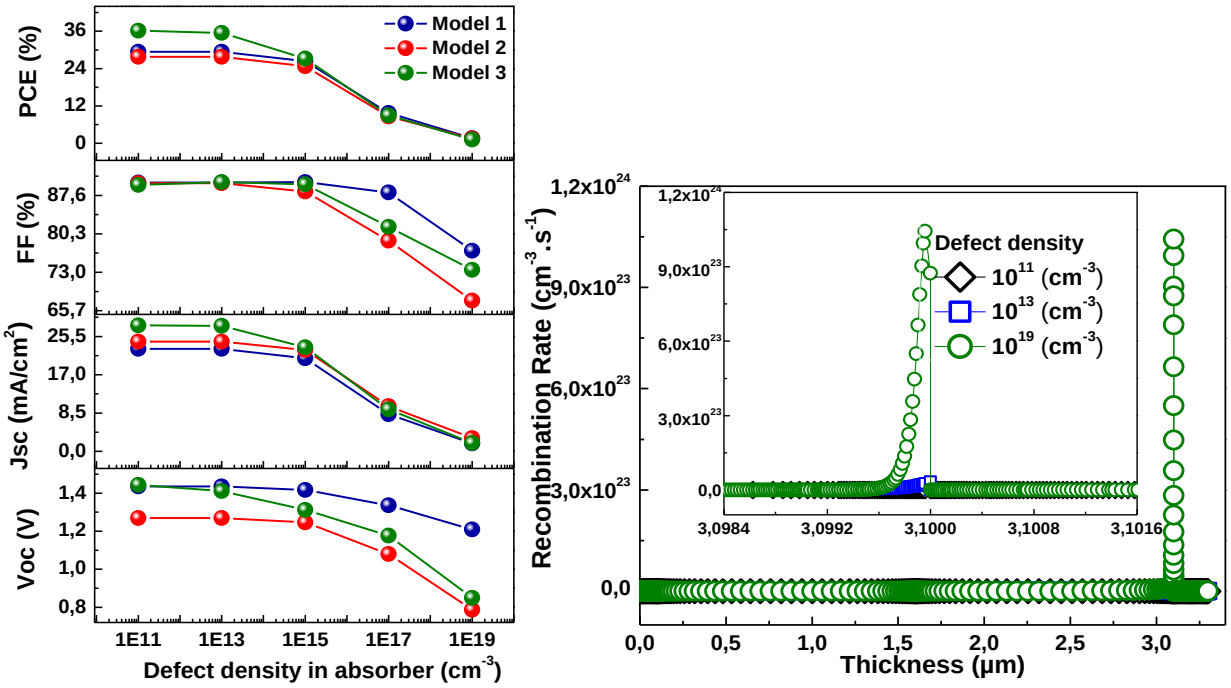

(a) (b)

Fig. 5 (a) Influence of defect density within the absorber of each cell on the I-V characteristics. (b) Influence of defect density in the absorber of the third cell on the recombination rate.

THE EFFECTS OF DEFECT DENSITY AT INTERFACES

The impact of defect density on the performance and durability of perovskite solar cells is a topic of increasing interest, with interfacial defects playing a critical role in charge carrier dynamics and recombination rates (Pochont et al., 2022;Thakur et al., 2022). This study delves into the intricate relationship between defect density and cell performance across three pivotal interfaces: MAPI/HTL, FAPI/MAPI, and ETL/FAPI.

At the MAPI/HTL interface, varying defect density from 10^{10} to 10^{18} cm^{-2} did not affect the J-V characteristics significantly. The Voc, Jsc, FF, and PCE remained stable across this range, with values of 1.414 V, 27.88 mA/cm^2, 90.98%, and 35.87%, respectively. Consequently, 10^{10} cm^{-2} was identified as the optimal defect density for the MAPI/HTL interface.

For the FAPI/MAPI interface, an increase in defect density led to a gradual decline in all photovoltaic parameters. Voc decreased from 1.413967 to 1.328337 V, Jsc from 27.88049576 to 24.1806729 mA/cm^2, FF from 90.9785 to 90.475%, and PCE from 35.8656 to 29.0606%. This decline was attributed to enhanced recombination, trapping, or scattering of charge carriers as they moved from the FAPI to the MAPI layer. The optimal defect density for this interface was determined to be 10^{10} cm^{-2}, resulting in improved performance metrics.

At the ETL/FAPI interface, an increase in defect density led to a reduction in all photovoltaic parameters. Voc decreased from 1.41 to 0.68 V, Jsc from 27.88 to 27.82 mA/cm^2, FF from 90.12 to 76.57%, and PCE from 35.46 to 14.43%. This decline was associated with a decrease in the number of collected charge carriers due to higher defect density in the ETL/FAPI interface (Bencherif and Hossain, 2022). The optimal defect density for this interface was found to be 10^{10} cm^{-2}, resulting in improved performance.

In summary, the comparison of these findings underscores the diverse effects of defect density on the three interfaces. While the FAPI/MAPI, and ETL/FAPI interfaces experienced performance declines with increasing defect density, the most significant impact was observed in the ETL/FAPI interface. In contrast, the MAPI/HTL interface exhibited consistent performance. Consequently, the study will concentrate on the double perovskite cell, which demonstrated superior performance under these conditions.

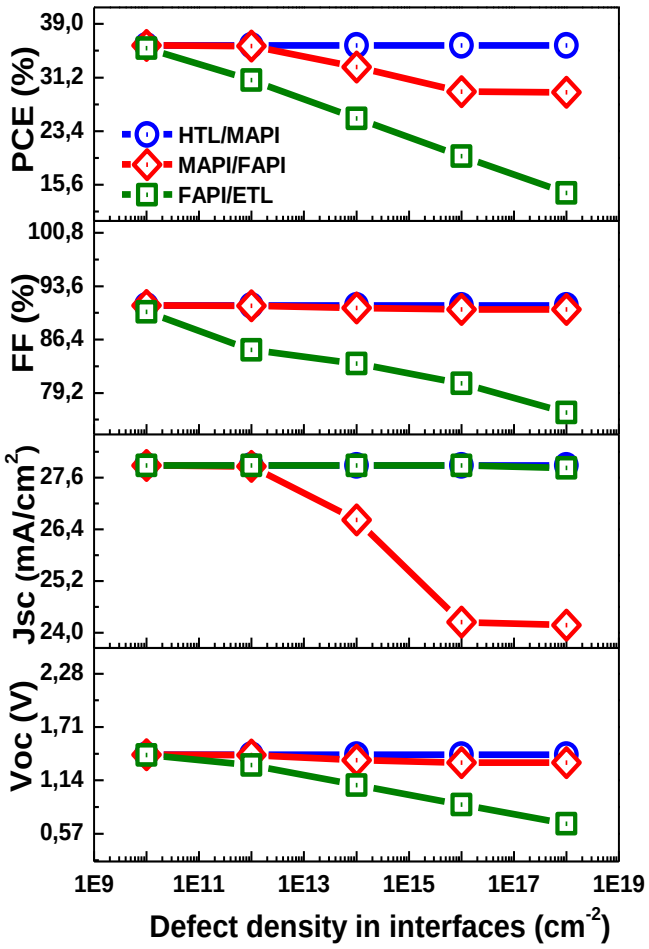

Fig.6. Influence of defect density in MAPI/HTL interface on the J-V characteristics.

CONCLUSION

In this study, three perovskite solar cell models were investigated using the SCAPS 1D simulator. The first two models were single-ply perovskite solar cells with FTO/ETL/MAPI/HTL/Pt and FTO/ETL/FAPI/HTL/Pt configurations, while the third model was a double absorber perovskite cell with the FTO/ETL/FAPI/MAPI/HTL/Pt configuration. After analyzing and comparing the impact of various parameters such as the thickness of the active layer, the doping and defect densities in the absorbing material for the three models, it was concluded that the double absorber cell had the potential to produce the best performance compared to the other two cells.

Furthermore, the study examined the effect of defect density in the three interfaces MAPI/ $CuSbS_2$, ZnO/FAPI and FAPI/MAPI, for the double absorber cell. The optimal defect density for these interfaces was found to be 10^{13} cm^{-2}, resulting in a Voc of 1.41 V, a Jsc of 27.88 mA/cm^2, an FF of 90.12%, and a PCE of 35.46% for an optimal thickness of 1500 nm, an acceptor doping density of 10^{20} cm^{-3}, and a defect density of 10^{10} cm^{-3} for each material (MAPI and FAPI) of the dual active layer.

The study of defect density and its impact on the performance of perovskite solar cells is a growing area of interest, with interfacial defects playing a crucial role in charge carrier dynamics and recombination rates. The research highlights the importance of understanding the influence of defect density on the performance of perovskite solar cells and the potential for optimization to improve their efficiency and longevity.

ACKNOWLEDGMENT

The SCAPS simulation program was a huge help to the authors and was provided by Prof. M. Burgelman and his colleagues at the Department of Electronics and Information Systems at the University of Gent in Belgium. The work is included in the PRFU project under contract number B00L02UN310220220001 Oran University of sciences and technology USTO-MB. www.mesrs.dz, and www.univ-usto.dz, http://www.prfu-mesrs.dz https://www.mendeley.com/impact/mostefa-benhalilibahttps://orcid.org/0000-0001-6507-3663

REFERENCES

Assirey, E. A. R. (2019). Perovskite synthesis, properties and their related biochemical and industrial application. *Saudi Pharmaceutical Journal*, *27*(6), 817-829.

Al-Mousoi, A. K., Mohammed, M. K., Pandey, R., Madan, J., Dastan, D., Ravi, G., & Sakthivel, P. (2022). Simulation and analysis of lead-free perovskite solar cells incorporating cerium oxide as electron transporting layer. *RSC advances*, *12*(50), 32365-32373.

Aseena, S., Abraham, N., & Babu, V. S. (2021). Optimization of layer thickness of ZnO based perovskite solar cells using SCAPS 1D. *Materials Today: Proceedings*, *43*, 3432-3437.

Bag, A., Radhakrishnan, R., Nekovei, R., & Jeyakumar, R. (2020). Effect of absorber layer, hole transport layer thicknesses, and its doping density on the performance of perovskite solar cells by device simulation. *Solar Energy*, *196*, 177-182.

Baral, P., Zhang, X., Garden, K., Chakraborty, N., Shen, L., Cao, Z., ... & Wang, H. (2023). Efficient and stable perovskite solar cells based on blade-coated CH3NH3PbI3 thin films fabricated using “green” solvents under ambient conditions. *Organic Electronics*, *116*, 106763.

Bencherif, H., & Hossain, M. K. (2022). Design and numerical investigation of efficient (FAPbI3) 1− x (CsSnI3) x perovskite solar cell with optimized performances. *Solar Energy*, *248*, 137-148.

Bera, S., Saha, A., Mondal, S., Biswas, A., Mallick, S., Chatterjee, R., & Roy, S. (2022). Review of defect engineering in perovskites for photovoltaic application. *Materials Advances*, *3*(13), 5234-5247.

Bouazizi, S., Tlili, W., Bouich, A., Soucase, B. M., & Omri, A. (2022). Design and efficiency enhancement of FTO/PC60BM/CsSn0. 5Ge0. 5I3/Spiro-OMeTAD/Au perovskite solar cell utilizing SCAPS-1D Simulator. *Materials Research Express*, *9*(9), 096402.

Chabri, I., Benhouria, Y., Oubelkacem, A., Kaiba, A., Essaoudi, I., & Ainane, A. (2023). Cs2AgBiBr6-based perovskite solar cell: A novel combination of

ITO/CdS/Cs2AgBiBr6/CuAlO2/Pt, with inorganic charge transport layers. *Optik*, *274*, 170560.

Chalapathi, U., Bhaskar, P. U., Cheruku, R., Sambasivam, S., & Park, S. H. (2023). Evolution of large-grained CuSbS2 thin films by rapid sulfurization of evaporated Cu–Sb precursor stacks for photovoltaics application. *Ceramics International*, *49*(3), 4758-4763.

Chowdhury, T. A., Zafar, M. A. B., Islam, M. S. U., Shahinuzzaman, M., Islam, M. A., & Khandaker, M. U. (2023). Stability of perovskite solar cells: issues and prospects. *RSC advances*, *13*(3), 1787-1810.

Daskeviciute-Geguziene, S., Zhang, Y., Rakstys, K., Xiao, C., Xia, J., Qiu, Z., ... & Nazeeruddin, M. K. (2023). Passivating Defects of Perovskite Solar Cells with Functional Donor-Acceptor–Donor Type Hole Transporting Materials. *Advanced Functional Materials*, *33*(1), 2208317.

De Los Santos, I. M., Cortina-Marrero, H. J., Ruíz-Sánchez, M. A., Hechavarría-Difur, L., Sánchez-Rodríguez, F. J., Courel, M., & Hu, H. (2020). Optimization of CH3NH3PbI3 perovskite solar cells: A theoretical and experimental study. *Solar Energy*, *199*, 198-205.

Dixit, H., Porwal, S., Boro, B., Paul, M., Ghosh, S., Mishra, S., & Singh, T. (2022). A theoretical exploration of lead-free double perovskite La2NiMnO6 based solar cell via SCAPS-1D. *Optical Materials*, *131*, 112611.

Hima, A., Lakhdar, N., Benhaoua, B., Saadoune, A., Kemerchou, I., & Rogti, F. (2019). An optimized perovskite solar cell designs for high conversion efficiency. *Superlattices and Microstructures*, *129*, 240-246.

Huang, S., Li, P., Wang, J., Huang, J. C. C., Xue, Q., & Fu, N. (2022). Modification of SnO2 electron transport Layer: Brilliant strategies to make perovskite solar cells stronger. *Chemical Engineering Journal*, *439*, 135687.

Husainat, A., Ali, W., Cofie, P., Attia, J., & Fuller, J. (2019). Simulation and analysis of methylammonium lead iodide (CH3NH3PbI3) perovskite solar cell with Au contact using SCAPS 1D simulator. *American Journal of Optics and Photonics*, *7*(2), 33.

Idrissi, S., Labrim, H., Bahmad, L., & Benyoussef, A. (2021). Study of the solar perovskite CsMBr3 (M= Pb or Ge) photovoltaic materials: Band-gap engineering. *Solid State Sciences*, *118*, 106679.

Karthick, S., Velumani, S., & Bouclé, J. (2020). Experimental and SCAPS simulated formamidinium perovskite solar cells: A comparison of device performance. *Solar Energy*, *205*, 349-357.

Ke, W., Stoumpos, C. C., & Kanatzidis, M. G. (2019). “Unleaded” perovskites: status quo and future prospects of tin-based perovskite solar cells. *Advanced Materials*, *31*(47), 1803230.

Kojima, A., Teshima, K., Shirai, Y., & Miyasaka, T. (2009). Organometal halide perovskites as visible-light sensitizers for photovoltaic cells. *Journal of the american chemical society*, *131*(17), 6050-6051.

Koné, K. E., Bouich, A., Marí-Guaita, J., Soucase, B. M., & Soro, D. (2023). Insight into the effect of halogen X in methylammonium lead halide (MAPbX3) spin-coated on zinc

oxide film. *Optical Materials*, *135*, 113238.

Lakhdar, N., & Hima, A. (2020). Electron transport material effect on performance of perovskite solar cells based on CH3NH3GeI3. *Optical Materials*, *99*, 109517.

Lye, Y. E., Chan, K. Y., & Ng, Z. N. (2023). A review on the progress, challenges, and performances of tin-based perovskite solar cells. *Nanomaterials*, *13*(3), 585.

Mushtaq, S., Tahir, S., Ashfaq, A., Bonilla, R. S., Haneef, M., Saeed, R., ... & Amin, N. (2023). Performance optimization of lead-free MASnBr3 based perovskite solar cells by SCAPS-1D device simulation. *Solar Energy*, *249*, 401-413.

Noman, M., Shahzaib, M., Jan, S. T., Shah, S. N., & Khan, A. D. (2023). 26.48% efficient and stable FAPbI 3 perovskite solar cells employing SrCu 2 O 2 as hole transport layer. *RSC advances*, *13*(3), 1892-1905.

Puente-López, E., & Pal, M. (2023). Numerical simulation and optimization of physical properties for high efficiency CuSbS2 thin film solar cells. *Optik*, *272*, 170233.

Pastuszak, J., & Węgierek, P. (2022). Photovoltaic cell generations and current research directions for their development. *Materials*, *15*(16), 5542.

Pochont, N. R., Sekhar, Y. R., Vasu, K., & Jose, R. (2022). Nitrogen-Doped Titanium Dioxide as a Hole Transport Layer for High-Efficiency Formamidinium Perovskite Solar Cells. *Molecules*, *27*(22), 7927.

Qasim, I., Ahmad, O., ul Abdin, Z., Rashid, A., Nasir, M. F., Malik, M. I., ... & Hasnain, S. M. (2022). Design and numerical investigations of eco-friendly, non-toxic (Au/CuSCN/CH3NH3SnI3/CdTe/ZnO/ITO) perovskite solar cell and module. *Solar Energy*, *237*, 52-61.

Qirong, Z., Bao, Z., Yongmao, H., Liang, L., Zhuoqi, D., Zaixin, X., & Xiaobo, Y. (2022). A study on numerical simulation optimization of perovskite solar cell based on CuI and C60. *Materials Research Express*, *9*(3), 036401.

Rai, N., Rai, S., Singh, P. K., Lohia, P., & Dwivedi, D. K. (2020). Analysis of various ETL materials for an efficient perovskite solar cell by numerical simulation. *Journal of Materials Science: Materials in Electronics*, *31*, 16269-16280.

Raj, A., Kumar, M., Kumar, A., Singh, K., Sharma, S., Singh, R. C., ... & Anshul, A. (2023). Comparative analysis of 'La'modified BiFeO3-based perovskite solar cell devices for high conversion efficiency. *Ceramics International*, *49*(1), 1317-1327.

Ravidas, B. K., Roy, M. K., & Samajdar, D. P. (2023). Investigation of photovoltaic performance of lead-free CsSnI3-based perovskite solar cell with different hole transport layers: First Principle Calculations and SCAPS-1D Analysis. *Solar Energy*, *249*, 163-173.

Rono, N., Merad, A. E., Kibet, J. K., Martincigh, B. S., & Nyamori, V. O. (2021). Optimization of Hole Transport Layer Materials for a Lead-Free Perovskite Solar Cell Based on Formamidinium Tin Iodide. *Energy Technology*, *9*(12), 2100859.

Shivesh, K., Alam, I., Kushwaha, A. K., Kumar, M., & Singh, S. V. (2022). Investigating the theoretical performance of Cs2TiBr6-based perovskite solar cell with La-doped BaSnO3 and CuSbS2 as the charge transport layers. *International Journal of Energy Research*, *46*(5), 6045-6064.

Sumbel, I., Raza, E., Ahmad, Z., Zubair, M., Mehmood, M. Q., Mehmood, H., ... & Rehman,

M. M. (2023). Numerical simulation to optimize the efficiency of HTM-free perovskite solar cells by ETM engineering.

Thakur, A., Singh, D., & Gill, S. K. (2022). Numerical simulations of 26.11% efficient planar CH3NH3PbI3 perovskite nip solar cell. *Materials Today: Proceedings*, *71*, 195-201.

Yang, S. J., Jin, H., Cha, J., Kim, M. K., Baek, D., Na, H., & Kim, M. (2023). Elucidating degradation mechanisms of mixed cation formamidinium-based perovskite solar cells under device operation conditions. *Applied Surface Science*, *612*, 155805.

Yousuf, R., & Qazi, G. (2021). Numerical modelling: Design and investigation of uniformly and non-uniformly doped absorber layer based PN homojunction perovskite solar cell variants. *Solar Energy*, *228*, 427-438.

Zahran, R., & Hawash, Z. (2022). Fullerene-Based Inverted Perovskite Solar Cell: A Key to Achieve Promising, Stable, and Efficient Photovoltaics. *Advanced Materials Interfaces*, *9*(35), 2201438.

Zhang, Y. N., Li, B., Fu, L., Zou, Y., Li, Q., & Yin, L. W. (2019). Enhanced optical absorption and efficient cascade electron extraction based on energy band alignment double absorbers perovskite solar cells. *Solar Energy Materials and Solar Cells*, *194*, 168-176.

Zhang, T., He, Q., Yu, J., Chen, A., Zhang, Z., & Pan, J. (2022). Recent progress in improving strategies of inorganic electron transport layers for perovskite solar cells. *Nano Energy*, *104*, 107918.

Zheng, D., Wang, G., Huang, W., Wang, B., Ke, W., Logsdon, J. L., ... & Facchetti, A. (2019). Combustion synthesized zinc oxide electron-transport layers for efficient and stable perovskite solar cells. *Advanced Functional Materials*, *29*(16), 1900265.